

# Supporting Information

Liu et al. 10.1073/pnas.1220912110

## SI Materials and Methods

**Fly Stocks and Genetics.** Six fly lines expressing the gene *egfp-bcd* (*bicoid*) *bcd* (1) were chosen as the founder lines for the generation of the Bcd-GFP fly line library (Table S1). Endogenous *bcd* in all founder lines was substituted by *bcd<sup>EL</sup>* mutant, which acts as a null allele (2). Among the six founder fly lines, one fly line termed 2X<sub>A</sub> with an X-chromosomal insertion of P[*egfp-bcd*] has been characterized in a previous study (1), and was chosen as our reference fly line. The other five fly lines were generated as follows: 2II<sub>A</sub> and 2II<sub>B</sub> were generated using P[*egfp-bcd*] in a  $\phi$ C31 RMCE integration vector (3) targeting the second chromosomal landing sites e38F1A and e43F9A, respectively; 2II<sub>C</sub> was generated by standard P-element-mediated transgenesis of P[*egfp-bcd*] and also chromosome II; and 2III<sub>A</sub> and 2III<sub>B</sub> were generated by mobilization of the original X-chromosomal Bcd-GFP transgene in fly line 2X<sub>A</sub> (1) on the third chromosome. The heterozygous fly lines with only a single copy of the *bcd* gene were generated by crossing females from the founder lines to males from fly line *yw*;+; *bcd<sup>EL</sup>*, *p<sup>UAS</sup>/TM3*. The fly lines with multiple insertions of P[*egfp-bcd*] were generated by crossing the founder lines with multiply balanced fly lines, such as *egfp-bcd*; *Sp/CYO*; *Dr/TMS, sb*. Oregon-R WT was used as a control in the live imaging experiment to measure the background. Fly lines mutant for the maternal factors Torso-like (Tsl) or Nanos (Nos) were generated by crosses between the Bcd-GFP fly lines to BNT(*yw*;+; *bcd<sup>EL</sup>* *nos<sup>BN</sup>* *tsl<sup>-</sup>/TMS, hs, sb*), BT(*yw*;+; *bcd<sup>EL</sup>* *tsl<sup>-</sup>/TMS, hs, sb*), and BN(*yw*;+; *bcd<sup>EL</sup>* *nos<sup>BN</sup>* *TMS, hs, sb*) (4–6). Note that these fly lines were extremely difficult to generate and to maintain, especially in backgrounds of higher than endogenous Bcd dosage. Progeny of these crosses were heat-shocked (37 °C for 1 h) on day 5 after egg deposition and allowed to develop at 22 °C. The surviving homozygous females were collected and set up onto egg collection plates for imaging experiments of their embryos.

**Live Imaging.** Embryo preparation for live imaging was as reported earlier (7), except that the mounting orientation was changed to the dorsal side facing up, closest to the imaging objective of an upright microscope. To reduce orientation variation during the mounting process, 200- $\mu$ m glass spacers were used to prevent mechanical stress when pushing the glass slide with glue on the embryos. Typically, the imaging for Bcd gradient measurement and cephalic furrow (CF) measurement was performed after  $16 \pm 2$  min and  $67 \pm 2$  min after entry into mitosis 13 (estimated by the disappearance of Bcd-GFP-filled nuclei), respectively. Live imaging was performed with a previously described custom-built, two-photon, point-scanning microscope (1), except that for fluorescence detection, a highly sensitive gallium-arsenide-phosphide (GaAsP) photomultiplier tube (module H10770PA-40 SEL; Hamamatsu) with dark counts smaller than 4,000 cps at 25 °C was used. The excitation wavelength was 970 nm, and average laser power at the specimen was 25 mW. Images were taken with a Zeiss 25 $\times$  (N.A. = 0.8) oil/water-immersion objective. Microscope control routines (8) and all our image analysis routines were implemented using MATLAB software (MathWorks). For each embryo, three images [512  $\times$  512 pixels, with 16 bits at 6.4  $\mu$ s per pixel (4 ms per line)] were taken along the anterior-posterior (AP) axis (focused at the midcoronal plane) at magnified zoom (linear pixel dimension corresponds to 0.46  $\mu$ m) and then stitched together in software; each image was an average of three sequentially acquired frames (Figs. 1A and 2A).

**Identification of Nuclei in Live Images.** The centroids of the nuclei were detected by searching for the peak intensity in a 7  $\times$  7-pixel

array around the center of the nuclear mask detected with a difference-of-Gaussian filter. The average nuclear fluorescence intensity was computed over a circular window of fixed size (diameter of 12 pixels). Embryos imaged at the midcoronal plane contained, on average, about 80 nuclei along each side, and roughly 60–70 of these nuclei could be detected automatically. The fluorescence background (green line in Fig. 1B) measured on WT embryos without Bcd-GFP expression is nearly zero and less than 20% of the nuclear Bcd-GFP fluorescence intensity at the posterior end. This low autofluorescence background is comparable to the dark counts in the image outside the embryo region.

**Bcd-GFP Dosage Measurements.** For each embryo, the nuclei detected from both sides were binned together with a bin size of 1% embryo length (EL) to obtain an average Bcd-GFP gradient along the AP axis for an individual embryo. To obtain the average Bcd-GFP gradient and its reproducibility for a given fly line, all nuclei detected in all embryos of the same fly line measured in a single imaging session were binned with a bin size of 1%EL, and the mean and SD for each bin were computed. Two types of dosage calculations were performed:

- The relative dosage of individual embryos was computed by a linear fit to the scatter plot of the single embryo gradient vs. the average Bcd-GFP gradient of the reference fly line 2X<sub>A</sub> measured in the same imaging session (Fig. 1D). To avoid fitting artifacts at the anterior and posterior poles, only data points within 10–80%EL were included in the fit.
- The average dosage of a fly line was computed by the linear fit to the scatter plot of the average Bcd-GFP gradient of that fly line vs. the average Bcd-GFP gradient of the reference fly line 2X<sub>A</sub> measured in the same imaging session (Fig. 1E and F).

For each dosage determination, measurements with at least 10 sample and 10 reference embryos were repeated over at least three independent imaging sessions. The mean value of the slopes was reported as the Bcd-GFP dosage of the sample fly line; its SD was determined by bootstrapping. The gradient intensity ratios of fly lines with different Bcd dosages remain constant over the time window from nuclear cycle (n.c.) 13 to late n.c. 14 (Fig. S3C); thus, relative Bcd dosages calculated with Bcd-GFP gradients measured 16 min after the start of n.c. 14 apply to the entire developmental process.

**Error Propagation for Arithmetic Test.** For the heterozygous fly lines derived from a founder fly line *A* with Bcd-GFP dosage  $|A| \pm \delta|A|$  (where  $\delta|A|$  is the measured SD), we computed the expected Bcd-GFP dosage and its SD as  $|A|/2 \pm \delta|A|/2$ . For a fly line generated by combining two different founder lines *A* and *B* with dosages  $|A| \pm \delta|A|$  and  $|B| \pm \delta|B|$ , respectively, the expected Bcd-GFP dosage of the fly line *A* + *B* is  $|A + B| \pm \sqrt{(\delta|A|)^2 + (\delta|B|)^2}$ , assuming the dosage measurements of the two founder lines are independent. The calculated expected Bcd-GFP dosages are shown as the horizontal error bars in Fig. 1G.

**Live Imaging Measurement Noise of Bcd-GFP Concentrations.** Gradient measurements are significantly improved over previous live imaging results (7) due to a substantial improvement of our imaging setup. This is demonstrated by the fact that we can detect nuclei containing Bcd-GFP all the way to the posterior end, which was not possible before, and by the fact that the embryo-to-embryo reproducibility in the anterior and posterior halves is at a

similar level. For inevitable residual experimental errors for Bcd dosage measurements, we identified six different sources of measurement noise:

- i-iii*) Imaging noise, nuclear identification noise, and focal plane adjustment noise as reported previously (7)
- iv*) Rotational asymmetry around the AP axis. Embryos are not rotationally symmetrical around the AP axis. To minimize the systematic error stemming from our inability to mount all embryos at the same azimuthal angle, we only selected embryos with near-perfect left-to-right symmetry that is given only in a dorsal view of the embryo, which was quantified by the intensity ratios between the left and right Bcd gradients. Only when this ratio was within 20% of unity did we retain the embryo for further analysis. The mean and SD of the ratios of the left and right gradients of the selected 968 embryos of reference fly line  $2X_A$  are  $0.94 \pm 0.05$ .
- v*) Rotational asymmetry around the left-to-right axis. Because the embryos were mounted on their curved ventral side, there was significant variability due to the rotational angle around the left-to-right axis. Misorientation stemming from this artifact can be easily spotted by faint membrane segments in the anterior and posterior pole regions. We identified three classes of embryos based on the range of these faint membrane segments: low (<1%EL), medium (<3%EL), and high (>3%EL). We only selected embryos that were devoid of such faint segments (low class), and we estimated the upper bound of the systematic measurement error due to this rotational angle to be of the order of 5% (i.e., the average deviation from unity of the relative dosage of individual embryos in the medium class).
- vi*) Sample size. Dosage measurements are typically made with sample sizes of at least 10 embryos per fly line per imaging session. For that case, the dosage measurement error is ~6% [using error propagation on the ratio of two fly lines with a SEM of 4% (as discussed in the main text) and assuming the measurement errors of the reference and sample fly line are independent].

**Live Imaging Measurement Noise of CF Positions.** For CF measurements (Fig. 2 *A* and *B*), we identified five different sources of measurement noise:

- i*) Measurement time uncertainty. The measured CF position shifts as development progresses are shown in Fig. S5*A*, and the estimated measurement error contributed from this source is ~0.35%.
- ii*) Focal plane adjustment noise. Measurements of CF positions in the z-stacks around the midcoronal plane (Fig. S5*B*) allowed us to estimate the measurement error from this source to be ~0.35%.
- iii*) Rotational around left-to-right axis. CF positions are independent of the rotational angle around the AP axis but depend on the rotation around the left-to-right axis. We classified embryos into three groups as described in the previous section. The upper bound for our CF measurement error from this source is 0.5%EL (the average deviation of the CF position of the medium class from the mean CF position of the low class).
- iv*) Nuclear shift. The nuclei shift posteriorly in the anterior region at the onset of CF formation. We estimated the measurement error from this source to be ~0.6%EL by quantifying the variance of the distance between the anterior tip of the embryo membrane and the anterior-most nuclei (Fig. S5*C*).
- v*) Image processing. CF locations were identified by manually clicking the center of the furrow gap (red dots in Fig. 2*A*). The resulting measurement error from this image processing step is ~0.23%EL (Fig. S5*D*).

**Antibody Staining and Confocal Microscopy.** All embryos were collected at 25 °C, heat-fixed, and labeled with fluorescent probes. Primary antibodies used were rat anti-Hunchback (Hb), guinea pig anti-Giant (Gt), rabbit anti-Krüppel (Kr), rabbit anti-Even-Skipped (Eve), and rabbit anti-Bcd (provided by Mark Biggins, Lawrence Berkeley National Laboratory, Berkeley, CA). Secondary antibodies used were Alexa Fluor 647 goat anti-rabbit IgG, Alexa Fluor 594 goat anti-guinea pig IgG, and Alexa Fluor 488 goat anti-rat IgG (AlexaFluor). For nuclear identification, all embryos were also stained with DAPI. Embryos were mounted in AquaPolymount (Polysciences, Inc.) with spacers between the slide and coverslip to minimize flattening. High-resolution digital images ( $1,024 \times 1,024$ , 12 bits per pixel) of fixed eggs were obtained on a Leica SP-5 confocal microscope with a  $20\times/0.7\text{-N.A.}/$  glycerol objective. The image focal plane was chosen at the midsagittal plane for protein profile extraction (Fig. S7*A*).

**Correction for EGFP Maturation in Live Bcd-GFP Measurements.** Because it takes tens of minutes for EGFP to mature, only a fraction of Bcd-GFP is visible in living embryos (9, 10). To obtain the actual Bcd-GFP concentration from the live Bcd-GFP measurement, we determined a maturation correction factor by fitting calculated Bcd-GFP gradients to measured Bcd-GFP gradients in both living and fixed embryos (Fig. S4 *A* and *B*). According to the synthesis-diffusion-degradation (SDD) model (1, 7, 11), the dynamics of the Bcd-GFP gradient can be described by  $\frac{\partial C_{tot}(x,t)}{\partial t} = D * \nabla^2 C_{tot}(x,t) - 1/\tau_d * C_{tot}(x,t) + j_0 \delta(x)$ , where  $C_{tot}(x,t)$  represents the total Bcd-GFP concentration, namely, the sum of the mature, visible Bcd-GFP ( $C_m(x,t)$ ) and immature, dark Bcd-GFP ( $C_{im}(x,t)$ ) in live Bcd-GFP measurements.  $D$  is the diffusion constant,  $\tau_d$  is the degradation time, and  $j_0$  is the Bcd-GFP synthesis rate. The steady-state solution of this equation is given by  $C_{tot}(x) = C_0 e^{-x/\lambda}$  with  $C_0 = j_0 / \sqrt{D/\tau_d}$  and  $\lambda = \sqrt{D * \tau_d}$ .  $C_{tot}(x)$  can be measured in fixed embryos, either directly with EGFP fluorescence (10) or after immunostaining for EGFP or Bcd (the latter is used in this work). For the immature Bcd-GFP contribution alone, the gradient dynamics also follow the SDD model except that  $1/\tau_d$  has to be replaced by  $1/\tau_d + 1/\tau_m$ , where  $\tau_m$  is the maturation time of EGFP. Thus, the steady-state gradient of immature Bcd-GFP is given by  $C_{im}(x) = C_0 * k * e^{-x/(k*\lambda)}$ , where  $k = \sqrt{\tau_m/(\tau_d + \tau_m)}$ . The Bcd-GFP contribution with mature EGFP follows from the difference  $C_m(x) = C_{tot}(x) - C_{im}(x)$ , and is the actual magnitude that is measured in living embryos. To determine the parameter  $k$ , we fit  $C_{tot}(x)$  and  $C_{im}(x)$  to the measured average Bcd-GFP gradients in fixed and living embryos from the reference fly line  $2X_A$ , respectively. The average Bcd-GFP gradients were calculated by selecting fixed embryos with the same orientation (dorsal view) and similar embryo age as the measured living embryos [ $16 \pm 5$  min into n.c. 14, determined by the invagination depth of the membrane furrow canals (12)]. At the chosen embryo age, Bcd-GFP gradients reach their steady state (1, 10). To reduce the number of fitting parameters, the background and amplitude of the raw intensity were corrected. The measured fluorescence intensity of Bcd-GFP can be described by  $I(x) = G * C(x) + B$ , where  $C(x)$  is the measured Bcd-GFP concentration,  $G$  is the imaging gain factor, and  $B$  is the imaging background.  $B$  was estimated for living embryos by measuring WT embryos under the same imaging conditions. For fixed embryos, we fitted the raw intensity profile of the gradient with the formula  $Ae^{-x/\lambda} + B$ . After background subtraction, the amplitudes of the gradients were adjusted by multiplying with a factor to match the gradient intensity in the posterior region ( $x/L = 0.8-0.9$ ), assuming that all Bcd-GFP molecules in that region have mature EGFP (Fig. S4*A*). We found that  $k = 0.7$  yields the best fit of the calculated gradients to their corresponding measured gradients:  $C_{tot}(x)$  vs. Bcd-GFP fixed and  $C_{im}(x)$  vs. Bcd-GFP live (Fig. S4*C*). The resulting  $\tau_d/\tau_m$  ratio is ~1, indicating

that the lifetime of Bcd-GFP is of the same order as the maturation time of EGFP in the embryo. Given the measured lifetime of Bcd-Dronpa [i.e.,  $\tau_d \cong 50\text{min}$  (9)], the above ratio implies that the maturation time of EGFP is  $\sim 50$  min, which is consistent within the range of currently estimated values in fly embryos (9, 13). Finally, the maturation correction factor for live Bcd-GFP measurement is given by  $R_M(x) = C_{tot}(x)/C_m(x)$ , using  $k = 0.7$  (Fig. S4D). It is an AP position-dependent factor with a maximum value of about 3 at the anterior pole and a minimum value of nearly 1 at the posterior pole.

**Determination of the Bcd-GFP Concentration at the CF Position.** The concentration at the location of the CF [ $C(x_{CF})$ ] can be expressed as  $C(x_{CF}) = C_D e^{-x_{CF}/\lambda}$ , where  $C_D$  and  $\lambda$  are the amplitude and length constants of the Bcd-GFP gradient, respectively. To calculate  $C(x_{CF})$ , several steps are necessary to convert the raw intensity of the Bcd-GFP gradient,  $I(x)$ , from live imaging to Bcd-GFP concentration  $C_{tot}(x)$ . First, the background  $B$  is subtracted from  $I(x)$  (see the section above). Then, the intensity is converted to Bcd-GFP concentration using the measured imaging gain factor  $G$ . Based on in situ Bcd-GFP concentration calibration (7),  $G = I_{ave}^R/8nM$ , where  $I_{ave}^R$  is the intensity of the average Bcd-GFP gradient of the reference fly line  $2X_A$  at location  $x/L = 0.48$ . The mature contribution ( $C_m$ ) of Bcd-GFP as measured with live imaging can be calculated as  $C_m(x) = (I(x) - B)/G$ . Finally, we used the maturation correction factor to calculate the total Bcd-GFP concentration  $C_{tot}(x) = C_m(x) * R_M$  (see the section above). We extracted  $C_D$  and  $\lambda$  from linear fits of  $\ln(C_{tot}(x))$  vs.  $x$ . Given the slope  $m$  and the intercept  $y_0$ ,  $\lambda = 1/m$  and  $C_D = \exp(y_0)$ . To avoid fitting artifacts at the anterior and posterior poles, only data points within the 20–80%EL range were included in the fits. The  $C(x_{CF})$  of all embryos of the sample fly line was normalized by  $C^R(x_{CF})$ , the mean value of  $C(x_{CF})$  of the reference fly line  $2X_A$ , measured in the same imaging session. Fig. 2C shows the relative  $C(x_{CF})$  vs. Bcd dosage  $D$ . As a control, we also extracted the concentration of nuclear Bcd-GFP  $C(x_{CF})$  at the location of the CF,  $x_{CF}$  from the corresponding Bcd-GFP concentration gradient by choosing the location of a measured nucleus closest to  $x_{CF}$  measured in the same embryo (Fig. S6A). Due to the measurement noise in both the determination of  $x_{CF}$  and the nuclear Bcd-GFP concentrations, the resulting SD on relative  $C(x_{CF})$  is  $16 \pm 5\%$  for the 19 sample fly lines, which is slightly higher than the  $14 \pm 4\%$  that we computed using  $C_D$  and  $\lambda$  from the fits. Nevertheless, we observe the same quasilinear relationship between the relative  $C(x_{CF})$  and Bcd dosage  $D$  on a log-log scale with both methods, with a slope  $S_c$  of  $44 \pm 2\%$  (Fig. 2C) and  $42 \pm 2\%$  (Fig. S6A), respectively.

#### Connection Between CF Position, Bcd Concentration, and Bcd Dosage.

How the CF position responds to the imposed Bcd dosage perturbations can be described either by a concentration representation [i.e.,  $C(x_{CF})$  vs.  $D$  (Fig. 2C and Fig. S6A)] or by a position representation [i.e.,  $x_{CF}$  vs.  $D$  (Fig. S6B)]. We can establish a mathematical connection between the two representations to show that the observed quasilinear relationship between  $\ln(C(x_{CF})/C^R(x_{CF}))$  and  $\ln(D)$  (see the section above) can be predicted from the quasilinear relationship  $x_{CF} = S_x \ln(D) + x_{CF}^R$ , as observed in Fig. S6B, where  $S_x$  is the slope of the linear fit. Combining this formula for  $x_{CF}(D)$  with  $C(x_{CF}) = C_D e^{-x_{CF}/\lambda}$ , and  $D = \frac{C_D}{C_D^R}$ , where  $C_D^R$  is the amplitude of the Bcd-GFP gradient of the reference fly line, we obtain  $C(x_{CF})/C^R(x_{CF}) = D^{S_c}$ , with  $S_c = 1 - \frac{S_x}{\lambda}$ . From our data, we infer that  $\lambda = 16.5 \pm 0.7\%$ EL and  $S_x = 10.5 \pm 0.2\%$ EL (dark solid line in Fig. S6B); thus, we predict that  $S_c = 36 \pm 2\%$ , which is very close to the measured value of the slope  $S_c = 44 \pm 2\%$  in Fig. 2C (dotted line). Most of the discrepancy between the two values comes from an  $\sim 10\%$  increase of  $\lambda$  as Bcd dosage  $D$  increases from 0.44 to 2.4 (Fig. S3A). Thus, the measured dependence between  $C(x_{CF})$  and Bcd dosage  $D$  is

quantitatively consistent with the measured dependence between  $x_{CF}$  and Bcd dosage  $D$ . This consistency also validates our calculation of  $C(x_{CF})$ , because we can derive its dependence on  $D$  directly from the raw data given by  $x_{CF}$  vs.  $D$  in Fig. S6B. With these two different representations, we demonstrate that the observed response of the CF position to Bcd dosage perturbations is quantitatively different from the two scenarios illustrated in Fig. S1. In the scenario following the traditional threshold-dependent readout model with  $S_c = 0$  in Fig. S1A, we have  $C(x_{CF}) = C^R(x_{CF})$ , and the Bcd concentration at  $x_{CF}$  is a constant (dashed line in Fig. 2C), corresponding to the linear relationship  $x_{CF} = \lambda nD + x_{CF}^R$  (dashed line in Fig. S6B). In the alternative scenario with  $S_c = 1$  (Fig. S1B), we have  $\frac{C(x_{CF})}{C^R(x_{CF})} = D$ , and the Bcd concentration at the CF location is proportional to the overall Bcd dosage (dashed-dotted line in Fig. 2C), corresponding to the constant function  $x_{CF} = x_{CF}^R$  (dashed-dotted line in Fig. S6B). Hence,  $S_c$  can be used as an indicator to quantify how much the Bcd concentration readout at a patterning marker's position deviates from the prediction of the threshold-dependent readout model. As for the CF, we can show that  $S_c$ , in fact, measures the percent reduction of the spatial CF shift with respect to the amount predicted by the threshold-dependent model. The actual shift of the CF is given by  $\Delta x_{CF} = x_{CF} - x_{CF}^R = S_x \ln D = \lambda(1 - S_c) \ln D$  (instead of  $\Delta x_{CF} = \lambda nD$ , as predicted by the threshold-dependent model). Thus, the observed shift is reduced by  $\lambda S_c \ln D$ , and the percentage of this reduction with respect to the predicted amount  $\lambda nD$  is  $S_c$ .

#### Quantification of Bcd-GFP Concentrations at Gene Expression Boundaries.

The Hb, Gt, Kr, and Eve protein profiles were extracted from confocal images of immunostained embryos using MATLAB software routines that allowed a rectangle window of the size of a nucleus to be systematically moved along the band of nuclei within the embryo as described previously (12). At each position, the average pixel intensity within the window was plotted vs. the projection of the window center along the AP axis of the embryo. The AP axis was defined as the major axis of the embryo mask. Protein profile measurements were made separately along the dorsal and ventral sides of the embryo (Fig. S7B). The boundaries of the Hb, Gt, and Kr anterior expression domains were detected at their location of half-maximal intensity with an estimated measurement error of  $\sim 0.6\%$  EL (Fig. S8A). Identification of seven local profile expression maxima determined the peak positions of Eve stripes. All automatically detected marker positions were manually verified (Fig. S8C). To minimize the measurement error from embryo orientation, marker positions were calculated as the average values of the positions from the dorsal and ventral sides for individual embryos (Fig. S8B) and only embryos imaged from a lateral view were chosen for data analysis. Embryo age was measured using the invagination depth of the membrane furrow canals during n.c. 14 (12). Under these stringent controls on embryo age and orientation, the SD of the Hb boundary and Eve peaks is less than 1%EL (Fig. S8), approaching the biological noise limit (12). Bcd-GFP concentrations at the detected marker positions were calculated with the same method as described above for  $C(x_{CF})$  except that we used the average Bcd-GFP gradient of the respective fly line [instead of the Bcd-GFP gradient of the corresponding single embryo as was the case for our  $C(x_{CF})$  calculations]. Given the high reproducibility of the Bcd-GFP gradients, the error in the thus calculated Bcd-GFP concentrations at these marker positions is less than 15%, which is well below the observed dynamic concentration changes between early and late time points in n.c. 14. Note that the changes of Bcd concentrations at the marker positions of these expression patterns are even smaller than in the case of the CF, and they evolve over time. Such small effects can only be revealed by a measurement protocol that is precise and accurate (i.e., where we understand the various sources of measurement noise) (12).



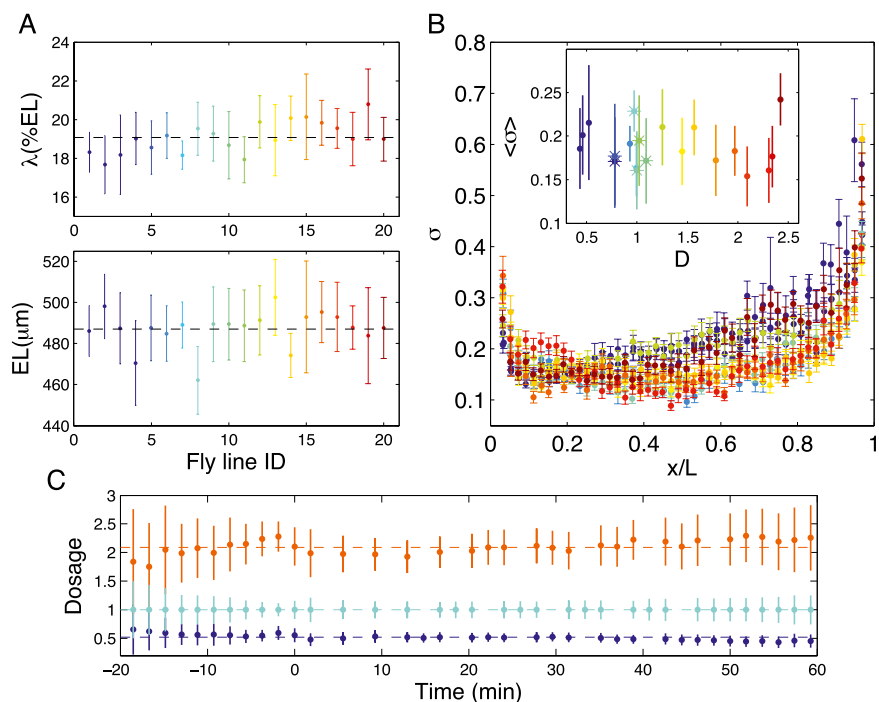


**Fig. S3.** Bcd-GFP gradient properties of 20 Bcd-GFP fly lines. (A) Means and SDs of the length constants  $\lambda$  (Upper) and embryo lengths (EL; Lower) of the sets of Bcd-GFP gradients of 20 Bcd-GFP fly lines listed in Table S1. The gradient length constants of the different lines are almost identical to the reference fly line with a mean and SD across the 20 fly lines of  $19.1 \pm 0.8\%$ EL. Note that in our live Bcd-GFP measurements, delayed EGFP maturation alters the shape of the Bcd gradient slightly. The mean length constant was reduced to  $16.5 \pm 0.7\%$ EL after corrections for EGFP maturation (*SI Materials and Methods*). (B) Relative variability of Bcd levels across embryos as a function of fractional embryo length for the 11 representative fly lines shown in Fig. 1F. The nuclei from 15 to 21 embryos per fly line were binned in 50 equidistant bins. The value of  $\sigma$  was calculated by dividing the SD of the nuclear intensity by the mean of each bin ( $\sigma = \delta[Bcd]/[Bcd]$ ). Error bars were computed by bootstrapping. Colors correspond to fly line identification (ID) nos. in A. (B, Inset) Reproducibility of  $\sigma$  averaged over a spatial region  $x/L = 0.2-0.8$  as a function of Bcd dosage  $D$  for 20 fly lines (ID nos. 1–20 in Table S1; founder lines are marked by stars). Error bars are SDs over that same region. Note the comparable levels of reproducibility across fly lines, guaranteeing the same measurement reliability for all dosages. (C) Time invariance of Bcd dosage measurements. Bcd dosages of fly line 1X<sub>A</sub> (blue; ID = 3) and fly line 2X<sub>A</sub>2III<sub>A</sub> (orange; ID = 16) are shown as a function of time; reference fly line 2X<sub>A</sub> (cyan; ID = 9) is measured concurrently for normalization. A time of 0 min is set at the onset of the 13th mitosis (evaluated by the disappearance of nuclear Bcd-GFP fluorescence). Error bars are SDs as described above. Dashed lines show the values of the expected dosage from measurement at 16 min.

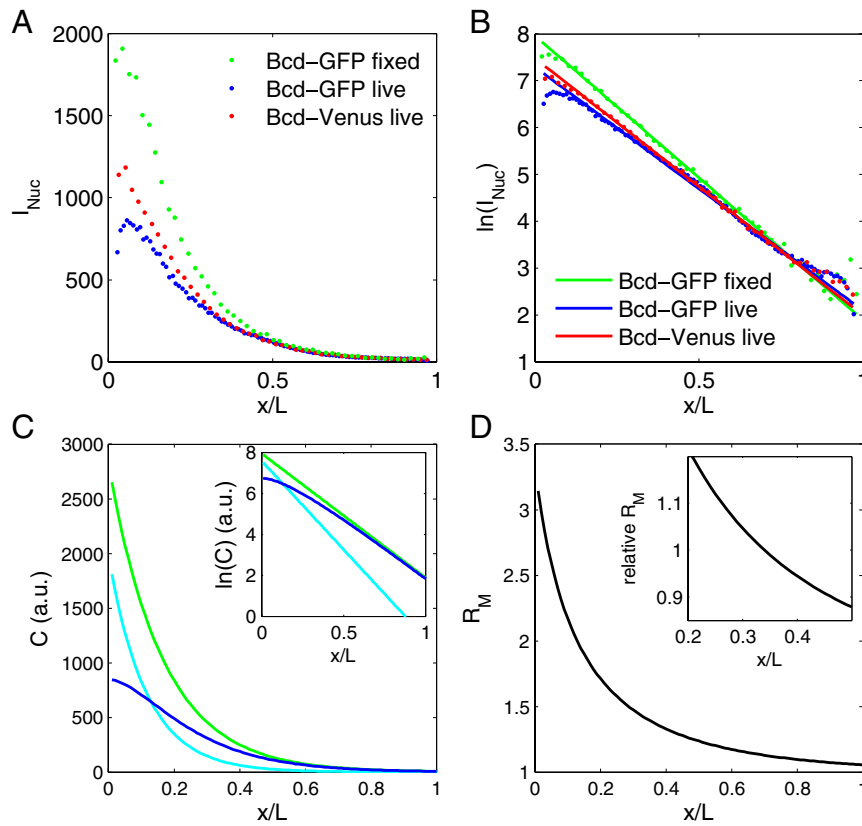


**Fig. S4.** EGFP maturation affects Bcd-GFP gradient measurements. (A) Comparison of  $I_{Nuc}$ , the binned nuclear fluorescence gradients averaged over 21 live  $2X_A$  embryos expressing Bcd-GFP (blue dots, from Fig. 1C), 27 live embryos expressing Bcd-Venus (red dots), and 12 fixed  $2X_A$  embryos immunostained for Bcd (green dots). (B) Log-linear ( $\ln$ ) plot of  $I_{Nuc}$  (fluorescence intensity of the Bcd gradients) vs.  $x/L$ . Colors for individual gradients are as in A. The length constants of the gradients obtained from linear fits to the data in the region  $x/L = 0.2-0.8$  are 19.3%EL (blue), 18.2%EL (red), and 16.4%EL (green), respectively. (C) Steady-state Bcd-GFP concentration  $C$  vs.  $x/L$ . The total concentration  $C_{tot}$  (green line) is composed of the  $C_m$  (blue line, contributed by Bcd-GFP molecules with matured EGFP, which are visible for live imaging) and the immature contribution  $C_{im}$  (cyan line, contributed by Bcd-GFP molecules with immature EGFP, which are invisible for live imaging), assuming the degradation time of Bcd-EGFP is the same as the maturation time of EGFP (*SI Materials and Methods*). (C, *Inset*) Log-linear plot of these gradients. a.u., arbitrary units. (D) Relative maturation correction factor  $R_M$  calculated as the ratio of the gradient of total Bcd-GFP (green line in C) to matured Bcd-GFP (blue line in C) (*SI Materials and Methods*). (D, *Inset*) Relative maturation correction factor in the region  $x/L = 0.2-0.5$  normalized by the maturation factor at the CF position of the reference fly line  $2X_A$ .









**Table S1. Fly line library with genetically modified Bcd dosages**

Fly line ID no.	Fly line name	Genotype	<i>D</i>	$x_{CF}$ (%EL)
1*	1II <sub>A</sub>	<i>yw; egfp-bcd/+; bcd<sup>E1</sup></i>	0.44 ± 0.03	25.1 ± 1.4
2	1II <sub>C</sub>	<i>yw; egfp-bcd/+; bcd<sup>E1</sup></i>	0.46 ± 0.04	27.7 ± 1.1
3*,†	1X <sub>A</sub>	<i>egfp-bcd/yw; +; bcd<sup>E1</sup></i>	0.52 ± 0.03	26.9 ± 1.3
4*,†	2II <sub>A</sub>	<b><i>yw; egfp-bcd; bcd<sup>E1</sup></i></b>	<b>0.78 ± 0.08</b>	<b>32.0 ± 1.3</b>
5	2II <sub>B</sub>	<b><i>yw; egfp-bcd; bcd<sup>E1</sup></i></b>	<b>0.78 ± 0.04</b>	<b>32.9 ± 1.0</b>
6*	1X <sub>A</sub> 1II <sub>A</sub>	<i>egfp-bcd/yw; egfp-bcd/+; bcd<sup>E1</sup></i>	0.93 ± 0.07	33.4 ± 1.1
7	1II <sub>A</sub> 1III <sub>A</sub>	<i>yw; egfp-bcd/+; egfp-bcd, bcd<sup>E1</sup></i>	0.97 ± 0.08	32.9 ± 0.7
8	2III <sub>A</sub>	<b><i>yw; +; egfp-bcd, bcd<sup>E1</sup></i></b>	<b>0.99 ± 0.17</b>	<b>33.6 ± 1.6</b>
9*,†	2X <sub>A</sub>	<b><i>egfp-bcd; +; bcd<sup>E1</sup></i></b>	<b>1.00 ± 0.06</b>	<b>34.4 ± 1.3</b>
10	2III <sub>B</sub>	<b><i>yw; +; egfp-bcd, bcd<sup>E1</sup></i></b>	<b>1.02 ± 0.07</b>	<b>32.8 ± 1.2</b>
11	2II <sub>C</sub>	<b><i>yw; egfp-bcd; bcd<sup>E1</sup></i></b>	<b>1.09 ± 0.05</b>	<b>34.2 ± 1.1</b>
12*	1X <sub>A</sub> 2II <sub>A</sub>	<i>egfp-bcd/yw; egfp-bcd; bcd<sup>E1</sup></i>	1.25 ± 0.10	37.4 ± 1.6
13*	2X <sub>A</sub> 1II <sub>A</sub>	<i>egfp-bcd; egfp-bcd/CYO; bcd<sup>E1</sup></i>	1.45 ± 0.09	38.2 ± 1.1
14*	2X <sub>A</sub> 2II <sub>A</sub>	<i>egfp-bcd; egfp-bcd; bcd<sup>E1</sup></i>	1.57 ± 0.13	40.0 ± 1.3
15	2II <sub>A</sub> 2III <sub>A</sub>	<i>yw; egfp-bcd; egfp-bcd, bcd<sup>E1</sup></i>	1.78 ± 0.13	41.4 ± 1.5
16*	2X <sub>A</sub> 2III <sub>A</sub>	<i>egfp-bcd; +; egfp-bcd, bcd<sup>E1</sup></i>	2.09 ± 0.14	41.4 ± 1.4
17	2X <sub>A</sub> 2III <sub>B</sub>	<i>egfp-bcd; +; egfp-bcd, bcd<sup>E1</sup></i>	2.12 ± 0.09	40.6 ± 1.0
18*	2X <sub>A</sub> 1II <sub>A</sub> 2III <sub>A</sub>	<i>egfp-bcd; egfp-bcd/CYO; egfp-bcd, bcd<sup>E1</sup></i>	2.31 ± 0.19	42.9 ± 1.5
19	2X <sub>A</sub> 2II <sub>A</sub> 2III <sub>A</sub>	<i>egfp-bcd; egfp-bcd; egfp-bcd, bcd<sup>E1</sup></i>	2.34 ± 0.18	45.0 ± 1.4
20*,†	2X <sub>A</sub> 2II <sub>C</sub> 2III <sub>A</sub>	<i>egfp-bcd; egfp-bcd; egfp-bcd, bcd<sup>E1</sup></i>	2.40 ± 0.17	43.0 ± 1.5
21 <sup>‡</sup>	1II <sub>A</sub> BNT	<i>yw; egfp-bcd/+; bcd<sup>E1</sup> nos<sup>BN</sup> tsI<sup>-</sup></i>	0.38 ± 0.06 <sup>§</sup>	19.3 ± 1.2
22 <sup>‡</sup>	1X <sub>A</sub> BNT	<i>egfp-bcd/yw; +; bcd<sup>E1</sup> nos<sup>BN</sup> tsI<sup>-</sup></i>	0.44 ± 0.06 <sup>§</sup>	22.5 ± 1.7
23 <sup>‡</sup>	1X <sub>A</sub> BT	<i>egfp-bcd/yw; +; bcd<sup>E1</sup> tsI<sup>-</sup></i>	0.47 ± 0.07 <sup>§</sup>	23.1 ± 1.0
24 <sup>‡</sup>	1X <sub>A</sub> BN	<i>egfp-bcd/yw; +; bcd<sup>E1</sup> nos<sup>BN</sup></i>	0.51 ± 0.06 <sup>§</sup>	28.0 ± 1.4
25 <sup>‡</sup>	2X <sub>A</sub> BNT	<i>egfp-bcd; +; bcd<sup>E1</sup> nos<sup>BN</sup> tsI<sup>-</sup></i>	0.82 ± 0.10 <sup>§</sup>	32.2 ± 1.3
26 <sup>‡</sup>	2X <sub>A</sub> BT	<i>egfp-bcd; +; bcd<sup>E1</sup> tsI<sup>-</sup></i>	0.94 ± 0.11 <sup>§</sup>	32.7 ± 1.0
27 <sup>‡</sup>	2X <sub>A</sub> BN	<i>egfp-bcd; +; bcd<sup>E1</sup> nos<sup>BN</sup></i>	0.99 ± 0.18 <sup>§</sup>	34.4 ± 1.3
28 <sup>‡</sup>	2X <sub>A</sub> 1II <sub>A</sub> BT	<i>egfp-bcd; egfp-bcd/+; bcd<sup>E1</sup> tsI<sup>-</sup></i>	1.33 ± 0.20 <sup>§</sup>	36.0 ± 1.6
29 <sup>‡</sup>	2X <sub>A</sub> 1II <sub>A</sub> BN	<i>egfp-bcd; egfp-bcd/+; bcd<sup>E1</sup> nos<sup>BN</sup></i>	1.35 ± 0.20 <sup>§</sup>	39.8 ± 1.6

Bcd dosages (*D*) and CF positions ( $x_{CF}$ ) are reported as population means with SDs; founder lines are marked in bold. BNT, *bcd-nos-tsI*; BT, *bcd-tsI*; ID, identification.

\*Eleven fly lines shown in Fig. 1F.

<sup>†</sup>Egg-hatching rates of fly lines 3, 4, 9, and 20 are 48%, 89%, 91%, and 67%, respectively. We were unable to generate fly strains that had Bcd dosages smaller than 0.44 or larger than 2.8. We believe these values correspond to the boundaries of viability. For all other generated fly lines, we obtained viable offspring, with hatching rates dropping for dosages close to these boundaries, consistent with earlier reports (1).

<sup>‡</sup>Nine maternal mutant fly lines shown in Fig. 4A. The only fly lines with maternal mutant backgrounds that we were able to generate are the ones shown here.

<sup>§</sup>The *nos* or *tsI* mutations slightly affect the nuclear Bcd compared with the same *egfp-bcd* insertions in a WT background. *TsI<sup>-</sup>* reduces Bcd dosage by about 10% (*D* of fly lines 23 vs. 3, 26 vs. 9, and 28 vs. 13) and the double mutation *tsI/nos* reduces the Bcd dosage by about 15% (*D* of fly lines 22 vs. 3, 21 vs. 1, and 25 vs. 9). The *nos* background alone does not appear to affect the Bcd dosage (*D* of fly lines 24 vs. 3, 27 vs. 9, and 29 vs. 13). These Bcd dosage differences with respect to WT are very close to our measurement error, and the mutant embryo sample sizes are much smaller than those for the Bcd-GFP fly lines in WT background. Therefore, it is uncertain whether the observed differences of Bcd dosages are statistically significant for our measurements.

1. Namba R, Pazdera TM, Cerrone RL, Minden JS (1997) *Drosophila* embryonic pattern repair: How embryos respond to bicoid dosage alteration. *Development* 124(7):1393–1403.